

Stage-parallel fully implicit Runge-Kutta implementations with optimal multilevel preconditioners at the scaling limit*

Peter Munch[†] Ivo Dravins[‡] Martin Kronbichler[§] Maya Neytcheva[‡]

15th June, 2022

Abstract

We present an implementation of a fully stage-parallel preconditioner for Radau IIA type fully implicit Runge–Kutta methods, which approximates the inverse of A_Q from the Butcher tableau by the lower triangular matrix resulting from an LU decomposition and diagonalizes the system with as many blocks as stages. For the transformed system, we employ a block preconditioner where each block is distributed and solved by a subgroup of processes in parallel. For combination of partial results, we either use a communication pattern resembling Cannon’s algorithm or shared memory. A performance model and a large set of performance studies (including strong scaling runs with up to 150k processes on 3k compute nodes) conducted for a time-dependent heat problem, using matrix-free finite element methods, indicate that the stage-parallel implementation can reach higher throughputs when the block solvers operate at lower parallel efficiencies, which occurs near the scaling limit. Achievable speedup increases linearly with number of stages and are bounded by the number of stages. Furthermore, we show that the presented stage-parallel concepts are also applicable to the case that A_Q is directly diagonalized, which requires complex arithmetic or the solution of two-by-two blocks and sequentializes parts of the algorithm. Alternatively to distributing stages and assigning them to distinct processes, we discuss the possibility of batching operations from different stages together.

Keywords— Implicit Runge-Kutta methods, Radau quadrature, stage-parallel preconditioning, finite element methods, matrix-free methods, geometric multigrid, massively parallel
MSC— 65Y05, 65M55, 68W10

1 Introduction

Runge–Kutta methods are widely used time-integration schemes to solve ordinary differential equations (ODE) of the form:

$$\frac{dy}{dt} = f(t, y).$$

*Dedicated to the memory of Owe Axelsson.

[†]Corresponding author. Helmholtz-Zentrum Hereon, University of Augsburg (peter.muench@uni-a.de).

[‡]Uppsala University (ivo.dravins/maya.neytcheva@it.uu.se).

[§]University of Augsburg, Uppsala University (martin.kronbichler@uni-a.de).

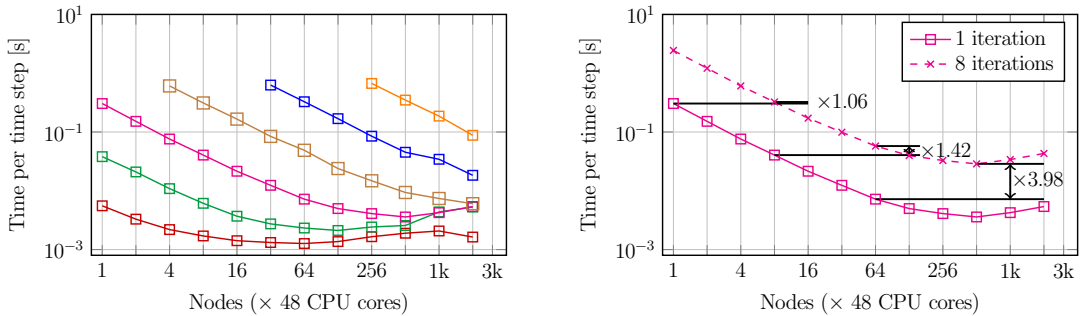


Figure 1: a) Time of a single conjugate gradient iteration preconditioned by GMG for different numbers of refinements $6 \leq L \leq 11$ and $k=1$. b) Example visualizing the benefit of stage parallelism for $Q=8$, by comparing the time of a single iteration with the one of eight iterations and providing idealized speedups in the case that Q iterations are solved in parallel by Q subgroups.

We consider a partial differential equation, rewritten as a system of ODEs after using finite element methods (FEM) to discretize in space. The basic algorithm is to obtain the solution at the next time step via linear combination of Q intermediate stage solutions:

$$\mathbf{y}_{n+1} = \mathbf{y}_n + \tau \sum_{1 \leq i \leq Q} b_i \mathbf{k}_i \quad \text{with} \quad \mathbf{k}_i = f(t_n + c_i \tau, \mathbf{y}_n + \tau \sum_{1 \leq j \leq Q} a_{ij} \mathbf{k}_j),$$

where t_n is the time at time step n and τ the current time-step size. The Butcher tableau is a compact notation for these methods in terms of a matrix A_Q as well as two vectors \mathbf{b}_Q and \mathbf{c}_Q .

There is a vast literature on optimizing Runge–Kutta methods. The investigations include improving the accuracy and the stability region as well as performance optimization. Low-storage Runge–Kutta methods [20], for instance, update the solution step by step so that the intermediate results for all stages need not be stored simultaneously, which might be an advantage for memory-intensive applications, e.g., computational plasma physics [27]. Implicit Runge–Kutta methods solve systems of increased size so that the development of efficient solvers is crucial [1, 5, 6, 9, 11, 12, 14, 19, 28, 29, 30].

In this work, we investigate solvers for fully implicit Runge–Kutta methods, focusing on the parallelization of the solution process of each stage [18]. Stage-parallel approaches and, similarly, parallel-in-time approaches [10, 25] (out of the scope of this work) are motivated by the scaling limit of algorithms, e.g., of iterative solvers, on distributed systems when parallelism is only exploited in the spatial domain. In the latter case, algorithms can not be run faster than a certain threshold even if more hardware resources are added. Figure 1a) shows, as an example, the times of one conjugate gradient iteration preconditioned by a single V-cycle of geometric multigrid (GMG) we will use in the experimental section when run across a large range of number of processes. It is clearly visible that the times flatten out when the work per process becomes too little. This phenomenon is also known as “scaling limit”. In the context of GMG, the minimum time of one iteration is approximately proportional to the number of levels. Since the total solution time of IRK is approximately the solution time accumulated over all stages run sequentially, the behavior of the overall solution time is similar under the assumption that each block corresponding to a stage can be solved by GMG.

As an alternative to the sequential solution process of each stage, one could assume that it is possible to solve the stages by Q process groups with GMG independently. In consequence, while the time for solving for one stage might take longer, the stages can be solved in parallel. A

speedup can be expected if the solution time of one stage does not increase significantly ($\ll Q$). Figure 1b) presents, as an example, the solution times for a single GMG iteration and for eight GMG iterations (assuming $Q=8$). In addition, it shows ideal speedups we can expect by solving one GMG iteration in parallel by each subgroup with one eighth of the processes. The speedup increases with increasing number of processes. Away from the scaling limit, the ideal speedup is only minor (a few percent), which will be dominated by organizational overheads in practice. At the scaling limit, the ideal speedup approaches Q . In summary, in the case that the IRK algorithm could be reformulated such that stages can be solved independently, this additional level of parallelism might allow to increase the granularity of the subproblem to solve and better utilize the capacity of the given hardware resources, such as to reach lower times to solution. In this publication, we show that such a reformulation is possible and, for a simple benchmark, we can achieve significant speedup at the scaling limit this way.

Stage-parallel implementations of implicit Runge–Kutta methods have been investigated but rarely implemented in the literature. One example is the work by Pazner and Persson [28], who considered a stage-parallel IRK preconditioner using a block-Jacobi solver across the processes around a local ILU: by solving the stages by subgroups of processes, the size of each block to be solved was increased and the efficiency of ILU was improved in terms of number of iterations so that speedups were reached. However, a critical discussion on the benefits of stage-parallel IRK regarding performance and on the challenges regarding efficient implementation in the context of more sophisticated global preconditioners and optimal preconditioners for the blocks, such as multigrid, are lacking in the literature.¹ In order to address this issue, we consider a direct factorization of the linear system arising from the implicit Runge–Kutta method and have extended a novel preconditioner for IRK, which has been introduced in [7]. Our results are based on benchmark programs leveraging the infrastructure of the open-source FEM library `deal.II` [3, 4] and are available on GitHub at <https://github.com/peterrum/dealii-spirk>.

As a critical remark, we note that running IRK and, generally, time-stepping schemes at the scaling limit means that the user has enough hardware resources and computational budget. Most scientists, however, are not in such a “luxurious” position. Hence, using stage-parallel Runge–Kutta methods and potentially parallel-in-time algorithms may not benefit them or might even be disadvantageous if applied far from the scaling limit due to some—unavoidable—organizational overhead.

The remainder of this contribution is organized as follows. Section 2 provides a short description of the linear systems arising from the implicit Runge–Kutta method and of stage-parallel solution procedures, followed by a discussion of their building blocks. Section 3 presents implementation details of the building blocks, and Section 4 discusses relevant performance models. Sections 5–6 demonstrate performance results for the solution of a time-dependent heat equation discretized by low- and high-order FEM with different stage-parallel solution procedures and compares them to results of non-stage-parallel versions of the solvers. Finally, Section 7 summarizes our findings and points to further research directions.

¹We define “optimal” as solver with high node-level performance whose number of iterations is independent of the number of DoFs and of the number of processes.

2 Fully implicit Runge–Kutta methods and stage-parallel solution approaches

In the following, we summarize key aspects of the implicit Runge–Kutta methods and stage-parallel solution procedures analyzed in this publication. We consider the subclass of implicit Runge–Kutta methods referred to as Radau IIA methods. For Q stages, the method order is given by $2Q-1$.

We restrict ourselves to the case of a linear system of equations of the form

$$M \frac{\partial \mathbf{u}(t)}{\partial t} + K \mathbf{u}(t) = \mathbf{g}(t),$$

where M denotes the mass matrix and K the stiffness matrix. To obtain the values of \mathbf{k}_q at the stages $q=1,\dots,Q$, we need to solve the system

$$\begin{bmatrix} M + \tau a_{11}K & \tau a_{12}K & \dots & \tau a_{1Q}K \\ \tau a_{21}K & M + \tau a_{22}K & \dots & \tau a_{2Q}K \\ \vdots & \vdots & \ddots & \vdots \\ \tau a_{Q1}K & \tau a_{Q2}K & \dots & M + \tau a_{QQ}K \end{bmatrix} \begin{bmatrix} \mathbf{k}_1 \\ \mathbf{k}_2 \\ \vdots \\ \mathbf{k}_Q \end{bmatrix} = \begin{bmatrix} K \mathbf{u}_0 + \mathbf{g}(t_0 + c_1\tau) \\ K \mathbf{u}_0 + \mathbf{g}(t_0 + c_2\tau) \\ \vdots \\ K \mathbf{u}_0 + \mathbf{g}(t_0 + c_Q\tau) \end{bmatrix},$$

which is expressed using Kronecker products as

$$(\mathbb{I}_Q \otimes M + \tau A_Q \otimes K) \mathbf{k} = \bar{\mathbf{g}} + (\mathbb{I}_Q \otimes K)(\mathbf{e}_Q \otimes \mathbf{u}_0).$$

Next, we multiply both sides by $(A_Q^{-1} \otimes \mathbb{I}_n)$ and use the relation $(A \otimes B)(C \otimes D) = (AC) \otimes (BD)$ to obtain

$$\underbrace{(A_Q^{-1} \otimes M + \tau \mathbb{I}_Q \otimes K)}_A \mathbf{k} = (A_Q^{-1} \otimes \mathbb{I}_n) \bar{\mathbf{g}} + (A_Q^{-1} \otimes K)(\mathbf{e}_Q \otimes \mathbf{u}_0), \quad (1)$$

which is the form we utilize in this study. Following Butcher [12], one can construct the spectral decomposition of $A_Q^{-1} = S \Lambda S^{-1}$ and use this to transform the matrix:

$$A = (A_Q^{-1} \otimes M + \tau \mathbb{I}_Q \otimes K) = (S \otimes \mathbb{I}_n)(\Lambda \otimes M + \tau \mathbb{I}_Q \otimes K)(S^{-1} \otimes \mathbb{I}_n).$$

The inverse of the matrix and the solution of the stages is explicitly given as:

$$\mathbf{k} = \underbrace{(S \otimes \mathbb{I}_n)(\Lambda \otimes M + \tau \mathbb{I}_Q \otimes K)^{-1}(S^{-1} \otimes \mathbb{I}_n)}_{A^{-1}} ((A_Q^{-1} \otimes \mathbb{I}_n) \bar{\mathbf{g}} + (A_Q^{-1} \otimes K)(\mathbf{e}_Q \otimes \mathbf{u}_0)). \quad (2)$$

In the context of Radau IIA methods, Λ is diagonal and contains $\lfloor Q/2 \rfloor$ complex-conjugate eigenvalue pairs as well as one real eigenvalue in the case of odd Q , and the matrix S contains the eigenvectors. Hence, $(\Lambda \otimes M + \tau \mathbb{I}_Q \otimes K)$ is block-diagonal and its inverse is given by the inverse of each block $(\lambda_i M + \tau K)$, which can be computed independently. In practice, one solves blocks corresponding to complex-conjugate eigenvalue pairs together, necessitating the solution of $\lfloor Q/2 \rfloor$ complex blocks via complex arithmetic or the transformation into two-by-two real blocks [30] and the solution of one real block in the case of odd Q .

In the literature, there are additional ways to factorize A_Q/A_Q^{-1} and to obtain a real block system more directly: The real Schur complement [29, 32] leads to block triangular matrices

\hat{S} , \hat{S}^{-1} and block diagonal matrix $\hat{\Lambda}$ with two-by-two blocks of the form $\begin{bmatrix} \Re(\lambda_i) & \alpha \\ -\Im(\lambda_i)^2/\alpha & \Re(\lambda_i) \end{bmatrix}$, for an arbitrary constant α .

Alternatively to factorizing \mathcal{A} directly, one can also solve the system (1) iteratively with a Krylov solver, like GMRES, with the help of a preconditioner. We note that for iterative solvers with suitable preconditioners, only the action of the matrix $(A_Q^{-1} \otimes M + \tau \mathbb{I}_Q \otimes K)$ on a vector has to be implemented, rather than the matrix itself.

Based on an observation in Axelsson [5], namely, that the matrix A_Q^{-1} has a dominating lower triangular part, Axelsson and Neytcheva [7] proposed to decompose $A_Q^{-1} = LU$. Here, matrix U has a unit diagonal, implying that all eigenvalues of $L^{-1}A_Q^{-1}$ are equal to one, which makes L suitable for constructing a preconditioner for (1). In order to obtain a preconditioner allowing for stage parallelism and real arithmetic, the spectral decomposition $L = \tilde{S}\tilde{\Lambda}\tilde{S}^{-1}$ is employed to construct the preconditioner. Its inverse is given as:

$$P^{-1} = (\tilde{S} \otimes \mathbb{I}_n)(\tilde{\Lambda} \otimes M + \tau \mathbb{I}_Q \otimes K)^{-1}(\tilde{S}^{-1} \otimes \mathbb{I}_n). \quad (3)$$

Just as before, the term $(\tilde{\Lambda} \otimes M + \tau \mathbb{I}_Q \otimes K)$ is block-diagonal and its inverse is given by the inverse of each block $(\tilde{\lambda}_i M + \tau K)$. The spectral decomposition of L is always real, which is the main motivation to use L instead of A_Q^{-1} . Hence, Q real blocks can be solved independently, in contrast to the complex case with only $\lceil Q/2 \rceil$ independent blocks. An analysis of the eigenvalues of the preconditioned system is provided in [6]. In the following, we drop the tilde over $\tilde{\Lambda}$ and \tilde{S} , as the meaning of these symbols is clear in the context they are used.

In (1), (2) and (3), one can identify multiple independent operations:

1. the right-hand-side function \mathbf{g} can be evaluated independently for each stage,
2. the matrix-vector multiplication with the mass matrix M and the stiffness matrix K in $(\mathbb{I}_q \otimes M)\mathbf{k}$ and $(\mathbb{I}_Q \otimes K)\mathbf{k}$ can be performed independently for each stage², and
3. Q or $\lceil Q/2 \rceil$ blocks involving $(\lambda_i M + \tau \otimes K)$ can be solved independently.

A parallel execution across the blocks/stages is a natural choice on modern supercomputers.

Obviously, the combination of the partial results from the stage-parallel execution via multiplication with $(A_Q^{-1} \otimes \mathbb{I}_n)$, $(S^{-1} \otimes \mathbb{I}_n)$ or $(S \otimes \mathbb{I}_n)$ is not independent. This step corresponds to a linear combination of the vector or, in the latter cases, to a basis change. Such an operation might be challenging in parallel, especially on distributed memory systems if each stage is assigned to a distinct process, and might counteract the benefits of the parallel execution of other parts of the algorithm.

In the following discussions of parallelization and implementation aspects, we omit the option of direct factorizing of \mathcal{A} , and consider it only in Section 6, pointing out that the proposed concepts are applicable in this context as well. For the realization of a stage-parallel iterative solver including the stage-parallel preconditioner, one needs an efficient parallel implementation of of basic tensor operations of the form from (1) and (3),

- “generalized vector scaling” with $C \in \mathbb{R}^{n \times n}$

$$\mathbf{v} = (\mathbb{I}_Q \otimes C)\mathbf{u} \quad \leftrightarrow \quad \mathbf{v}_i = C\mathbf{u}_i \quad (4)$$

²Note that the following decomposition is applicable: $A_Q^{-1} \otimes M = (A_Q^{-1} \otimes \mathbb{I}_n)(\mathbb{I}_Q \otimes M)$.

- “generalized matrix-vector product” with $D \in \mathbb{R}^{Q \times Q}$

$$\mathbf{v} = (D \otimes \mathbb{I}_n) \mathbf{u} \quad \leftrightarrow \quad \mathbf{v}_i = \sum_{1 \leq j \leq Q} D_{ij} \mathbf{u}_j. \quad (5)$$

Furthermore, we analyze the benefits of the stage-parallel solver in comparison to its sequential counterpart. For the blocks, we use geometric multigrid [26] as efficient solver with state-of-the-art parallel scaling.

We call the algorithm (1)+(3) *stage-parallel IRK* (in the figures abbreviated as *SPIRK*) when the blocks are solved in parallel. When the blocks are solved sequentially, we simply use *IRK*.

We conclude this section by providing a brief comparison of the preconditioner (3) and the ones considered by Pazner and Person [28] solving time-dependent non-linear problems. They analyze block Jacobi solvers with different block sizes: one that takes into account all coupling terms between stages (“stage-coupled”) and one that ignores them (“stage-uncoupled”). In the latter case, the blocks corresponding to the stages are independent of each other and can be solved in a stage-parallel way. The structure is very similar to the inner term of (3). However, we note that the basis changes \tilde{S} and \tilde{S}^{-1} imply a coupling of the stages. We show that the cost of the basis changes is small, enabling a stage-parallel “stage-coupled” preconditioner with the cost similar to that of the stage-parallel “stage-uncoupled” preconditioner proposed in [28].

3 Implementation details

In the following, we discuss pure MPI implementations of the stage-parallel IRK; in some of our experiments, we use MPI’s shared-memory features. The algorithms can be easily generalized to task-based implementations, as provided by OpenMP, and to hybrid implementations (MPI+X). In Sections 3.1–3.3, we describe an approach where stages are distributed and assigned to distinct processes, and, in Section 3.4, we describe a way to batch operations from different stages. Both approaches aim to increase the parallelism in the solver and hereby to increase the sizes of the subproblems that can be processed in parallel.

3.1 Domain decomposition

We decompose the mesh of our spatial computational domain into B partitions. In the case of IRK, we assign each partition to a (MPI) process. In the case of stage-parallel IRK, we assign each process a pair $(q, b) \in [1, Q] \times [1, B]$ consisting of a stage and a partition. For the sake of simplicity, we enumerate the processes lexicographically, as shown in Figure 2. However, a basic preprocessing step based on virtual topologies allows us to use any enumeration of processes, as is needed in later discussions.

In total, we need at least $Q \times B$ processes. In order to be able to perform operations between processes with the same stage (e.g., to solve the inner blocks) or the same partition (e.g., for the basis change), we use additional subcommunicators: `column_comm` and `row_comm`. This is a common approach in the context of distributed matrix-matrix-multiplication implementations [31] and finite-difference stencil computations on Cartesian meshes [17]. A similar approach has been used in [27] to solve the 6D Vlasov–Poisson equation on the tensor product of a 3D geometric domain and a 3D velocity-space domain.

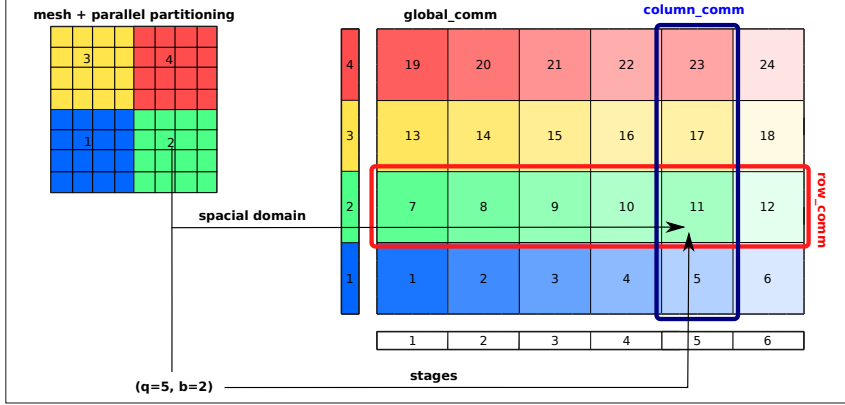


Figure 2: Three MPI communicators (for a hypothetical setup with 24 processes, $Q=6$ stages, and $B=4$ partitions) used to simplify communications in stage-parallel IRK: `global_comm` collects processes with work and `column_comm/row_comm` collects processes owning the same stage/partition of the computational domain. Furthermore, the mapping between the stage/partition pair and the rank in the global communicator is indicated. Adopted from [27].

3.2 Parallel data distribution

A natural choice is to let each process (q,b) own the locally relevant part of the vectors associated with the stage q and let it update the locally owned part of the solution vector during evaluation of the right-hand-side function, of the matrix-vector product, and of the block solvers.

For the operation $\mathbf{v} = (\mathbb{I}_Q \otimes C)\mathbf{u}$, setting $\mathbf{v}_q = C\mathbf{u}_q$ does not require communication between stages. However, each process needs access to the local part of the matrix $C \in \mathbb{R}^{n \times n}$ (in our case: M and K). The need for local access to the matrix means that certain data structures have to be duplicated Q times on distributed systems. This could be addressed by using shared memory. Since all our experiments are run without assembling any matrix (“matrix-free approach”), which is memory-efficient [22], we defer its investigation to future work.

In contrast, the operation $\mathbf{v} = (D \otimes \mathbb{I}_n)\mathbf{u}$ only needs access to a small matrix $D \in \mathbb{R}^{Q \times Q}$, which can easily be replicated on all processes. The major challenge for this operation is that a process needs to access the local vector entries of all stages, e.g., $\mathbf{v}_2 = D_{11}\mathbf{u}_1 + D_{21}\mathbf{u}_2 + \dots + D_{2Q}\mathbf{u}_Q$. The gathering of the needed vector entries from all stages is not feasible as this would mean that the vectors are duplicated Q -times. In the next sections, we discuss an appropriate communication pattern to alleviate this problem and compare its performance to the one of a shared-memory approach, in which the processes have direct read access to the needed entries of all stages.

3.3 Distributed tensor operations

To derive a memory-efficient implementation of the operation $\mathbf{v} = (D \otimes \mathbb{I}_n)\mathbf{u}$, which is needed for the linear combinations during the setup of the right-hand-side vector and during the matrix-vector multiplication as well as for the basis changes, one can exploit its associativity:

$$\begin{bmatrix} \mathbf{v}_1 \\ \mathbf{v}_2 \\ \vdots \\ \mathbf{v}_Q \end{bmatrix} = \underbrace{\begin{bmatrix} D_{11}\mathbf{u}_1 \\ D_{21}\mathbf{u}_1 \\ \vdots \\ D_{Q1}\mathbf{u}_1 \end{bmatrix} + \begin{bmatrix} D_{12}\mathbf{u}_2 \\ D_{22}\mathbf{u}_2 \\ \vdots \\ D_{Q2}\mathbf{u}_2 \end{bmatrix} + \dots + \begin{bmatrix} D_{13}\mathbf{u}_3 \\ D_{23}\mathbf{u}_3 \\ \vdots \\ D_{Q3}\mathbf{u}_3 \end{bmatrix}}_{\mathbf{v}_i = \sum_j D_{ij}\mathbf{u}_j} = \underbrace{\begin{bmatrix} D_{11}\mathbf{u}_1 \\ D_{22}\mathbf{u}_2 \\ \vdots \\ D_{QQ}\mathbf{u}_Q \end{bmatrix} + \begin{bmatrix} D_{12}\mathbf{u}_2 \\ D_{23}\mathbf{u}_3 \\ \vdots \\ D_{Q1}\mathbf{u}_1 \end{bmatrix} + \dots + \begin{bmatrix} D_{13}\mathbf{u}_3 \\ D_{24}\mathbf{u}_4 \\ \vdots \\ D_{Q(Q-1)}\mathbf{u}_{(Q-1)} \end{bmatrix}}_{\mathbf{v}_i = \sum_k D_{ik}\mathbf{u}_k \text{ with } j := (i+k)\%Q} \quad (6)$$

If we consider each summand as a computation step, we see that each process needs access to a different part of the source vector \mathbf{u} associated with a stage. In order to obtain the right data access, the communication pattern is as follows. After each computation step, the matrix is rotated to the left and the source vector upwards. The algorithm is similar to Cannon’s algorithm [13], which is designed for distributed matrix-matrix multiplications. In contrast to Cannon’s algorithm, we operate on tensors and with fully replicated D . In the case that \mathbf{u} is distributed, we get a circular communication pattern, which can be built around a sequence of calls to `MPI_Sendrecv_replace`, operating on `comm_row`.

3.4 Batching of operations

Sections 3.1–3.3 consider an approach that also employs parallelism across the stages by assigning each stage to a distinct compute unit. For fixed computational resources and problem sizes, this increases the size of the spatial subproblems and reduces the number of communication steps. Alternatively, one could increase the local work by processing Q stages on the same compute unit in a batched fashion. To be efficient, all operations of the form $\mathbf{v} = (\mathbb{I}_Q \otimes C)\mathbf{u}$ in (1) and of the solvers of the steps in (3) need to support this matrix-times-multivector mode of processing.

For the geometric multigrid solver used for the experiments in Sections 5 and 6, all ingredients in terms of smoother, prolongator/restrictor, and coarse-grid solver need to support batching. For simple smoothers and coarse-grid solvers, like Chebyshev iterations around a point-Jacobi method, this is the case, whereas it is typically not the case for algebraic multigrid.

Batching is more efficient in terms of memory consumption, since shared data structures, particularly the matrices M and K , only need to be stored once. Furthermore, also data structures pertaining to matrix-free evaluation need to be loaded once per iteration. For instance, many matrix-free implementations load the mapping data, e.g., the Jacobian matrix of size $\mathbb{R}^{3 \times 3}$ in 3D, for each quadrature point during cell loops. On affine meshes, the mapping data is the same at each quadrature point so that it can be re-used from fast caches [22, 23]. However, no simple compression is available for deformed mesh cells, where matrix-free loops become memory-bound on modern hardware. In a sequential execution of the stage solvers, the mapping data has to be loaded from main memory for each stage. Also for stage parallelism according to Sections 3.1–3.3, different processes load separate arrays via a shared resource, the bus from main memory, again giving a similar cost as in the stage-sequential case. In contrast, batching allows to load the mapping data once, since all stages are processed during a single cell loop where data from caches is still hot. Additional work for evaluating the cell integrals of multiple stages could be hidden behind the slow memory access.

As an alternative, on-the-fly evaluation of high-order mappings for complicated geometries is possible [24], but it comes with additional complexities. We therefore concentrate on affine meshes in this work and defer the investigation of complicated meshes in the context of stage parallelism to future work.

4 Performance modeling

In the following, we derive performance models for sequential and stage-parallel IRK. Since the application of the preconditioner P^{-1} is the most expensive ingredient in both cases (see the results in Section 5), we consider it in detail. The statements made for the preconditioner can be straightforwardly transferred to other parts of the algorithm.

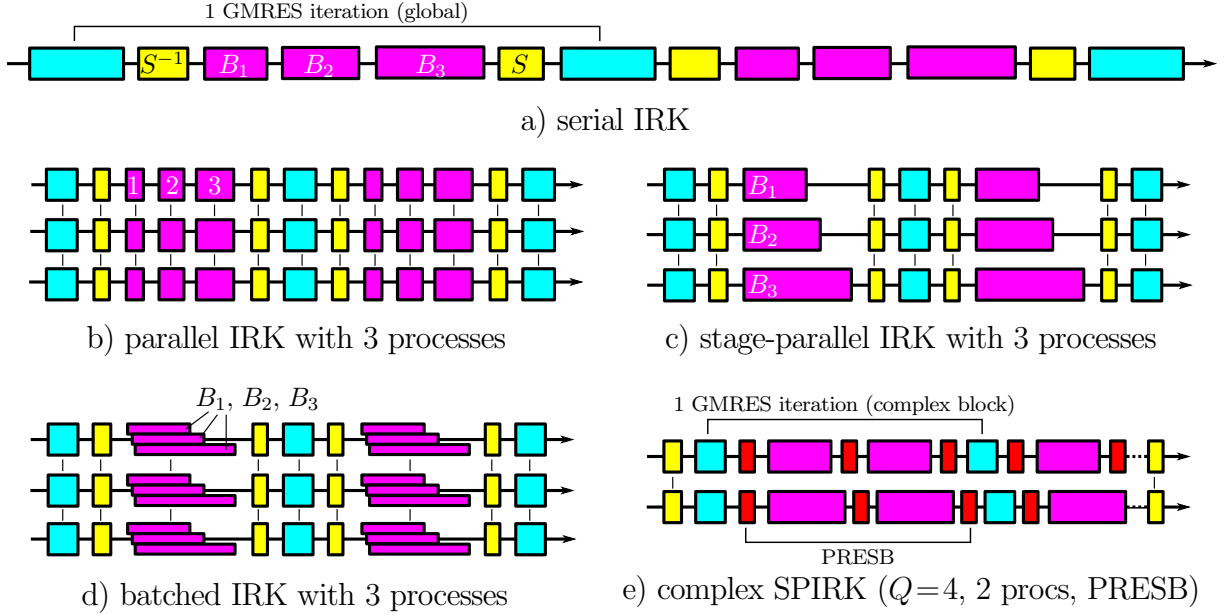


Figure 3: a-d) Visualization of a serial, a parallel, a stage-parallel, and a batched execution of the application of preconditioner P^{-1} of IRK with $Q=3$. The main components are the GMRES solver, the basis changes (S , S^{-1}), and the block solvers (B_i). e) Visualization of a stage-parallel execution of the complex IRK with $Q=4$ and PRESB. Vertical lines indicate communication between processes.

Figure 3a) shows a possible trace of a serial execution of IRK, and Figure 3b) presents a parallel execution of IRK (with 3 processes). In both cases, the basis change S^{-1} , the inner block solvers B_i , and the basis change S are executed in sequence so that one gets for the total runtime of the application of the preconditioner:

$$T_{\text{IRK}}(N) = 2 \cdot T_S(N) + \sum_{1 \leq q \leq Q} T_{B_i}(N), \quad (7)$$

where $T_{\text{IRK}}(N)$ denotes the total time for one application of the preconditioner. Clearly, it is a function of the number of processes N . In the ideal case, $\mathcal{T}_{\square}(N) \approx T_{\square}(1)/N$. However, inherently serial parts in the code prevent perfect scaling.

In the stage-parallel case, the steps of the inner block solver are performed in parallel. Since each block may have different properties, the solution processes might take different amounts of time and require different numbers of inner iterations in the case that iterative solvers are used on the blocks. Recall that the block systems are of the form $(\lambda_i M + \tau K)$, the number of stages slightly affects the range of values of λ_i , the discretization affects the entries of M , and the time step τ scales the stiffness matrix K .

The solution of each block is combined during the application of S , leading to an unavoidable synchronization. This results in a trace, as indicated in Figure 3c), and in a total runtime that is determined by the maximum runtime of any of the block solvers:

$$T_{\text{SPIRK}}(N) = 2 \cdot T'_S(N) + \max_{1 \leq q \leq Q} (T_{B_q}(N/Q)). \quad (8)$$

Equation (8) also describes the runtime in the case of the batched approach (see Figure 3d)).

Table 1: Number of cells and of degrees of freedom for different number of refinements L .

L	cells	degrees of freedom		L	cells	degrees of freedom	
		$k=1$	$k=4$			$k=1$	$k=4$
4	4.1E+03	4.9E+03	2.7E+05	8	1.7E+07	1.7E+07	1.1E+09
5	3.3E+04	3.6E+04	2.1E+06	9	1.3E+08	1.4E+08	8.6E+09
6	2.6E+05	2.7E+05	1.7E+07	10	1.1E+09	1.1E+09	6.9E+10
7	2.1E+06	2.1E+06	1.4E+08	11	8.6E+09	8.6E+09	5.5E+11

Based on (7) and (8), one can expect the following parallel performance behavior. The timings are comparable if 1) T_S and T'_S are of the same order, 2) the block solvers are scaling nearly ideally, i.e., $T_{B_i}(N) \approx T_{B_i}(1)/N$, and 3) the solution times of the block solvers are comparable, i.e., $\forall i \neq j: T_{B_i} \approx T_{B_j}$. The parallel performance of the sequential IRK deteriorates if $T_{\square}(N) \gg T_{\square}(1)/N$, which is the case at the scaling limit. The performance of the stage-parallel IRK method deteriorates if there is a significant difference in the solution times of the block solvers, limiting the maximum speedup to $\sum_Q T_{B_q} / \max(T_{B_q}) \leq Q$. One can deduce that stage-parallel IRK has advantages only if IRK is at the scaling limit and the solution times of the blocks are comparable.

In the discussion above, we assumed wall-clock times of the solution of a block as given. However, we can refine the expressions for iterative solvers:

$$T_{\text{IRK}}(N) = \sum_{1 \leq q \leq Q} N_i^{\text{IT}} \cdot \hat{T}_{B_i}(N) \quad \text{and} \quad T_{\text{SPIRK}}(N) = \max_{1 \leq q \leq Q} \left(N_q^{\text{IT}} \cdot \hat{T}_{B_q}(N/Q) \right),$$

with \hat{T}_i being the time of one iteration and N_i^{IT} the number of iterations. For the sake of simplicity, T_S and T'_S are dropped. If we assume that we are at the scaling limit ($\lim_{N \rightarrow \infty} \hat{T}_q(N) \approx \lim_{N \rightarrow \infty} \hat{T}_q(N/Q)$), we get the expressions:

$$\lim_{N \rightarrow \infty} T_{\text{IRK}}(N) \sim \sum_{1 \leq q \leq Q} N_i^{\text{IT}} \quad \text{and} \quad \lim_{N \rightarrow \infty} T_{\text{SPIRK}}(N) \sim \max_{1 \leq q \leq Q} (N_q^{\text{IT}}),$$

indicating that it is possible to estimate bounds of maximum speedups based on the number of iterations that can be run in parallel. This gives also a simple mean to compare the benefits to alternative (stage-parallel) implementations, like the direct factorization (2), where one could consider all block solves accumulated over all GMRES iterations for one time step.

In the numerical experiments in Section 5 and 6, we will evaluate the statements made above.

5 Numerical experiments

In this section, we present performance results of the stage-parallel implementation of (1)+(3). We start with results obtained on 16 compute nodes. In particular, we discuss the performance of a base configuration and the influence of key parameters. We conclude the section with presenting a strong-scaling analysis.

Hereafter, we solve the 3D heat problem $\partial u / \partial t = \Delta u + f$ with the following manufactured solution:

$$u(x, y, z, t) = \sin(2\pi x) \sin(2\pi y) \sin(2\pi z) (1 + \sin(\pi t)) \exp(-0.5t),$$

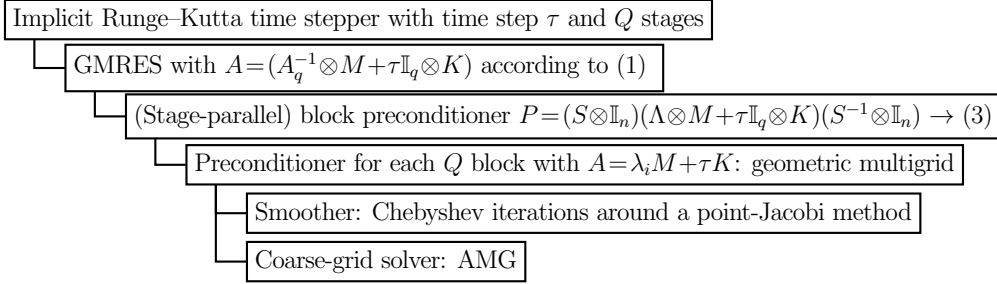


Figure 4: Diagram of the solver used to solve the heat problem in Section 5.

on a cube $\Omega = [0,1]^3$. The source-term function f and the Dirichlet boundary conditions are selected appropriately. The spatial variables are discretized with the finite element method, for which we use the open-source library `deal.II` [3, 4]. The mesh is obtained by L steps of isotropic refinement of a coarse mesh consisting of a single hexahedral cell, giving 2^L mesh cells per spatial direction or 2^{3L} cells in total. We use continuous Lagrange finite elements, defined as the tensor products of 1D finite elements with degree k . For quadrature, we consider the consistent Gauss–Legendre quadrature rule with $(k+1)^3$ points. Table 1 shows the number of cells and the number of degrees of freedom for $k=1$ and $k=4$ for $4 \leq L \leq 11$. The time step is set to $\tau=0.1$, and we run 10 time steps.

As outer solver of (1), we apply GMRES. It is run until the l_2 -norm of the residual has been reduced by 10^{12} . As approximate inverse of each block of (3), we use a single V-cycle of the geometric multigrid from `deal.II` [26]. As a smoother, we apply Chebyshev iterations around a point-Jacobi method [2] with degree 5 and, as coarse-grid solver, we use the algebraic multigrid solver from ML [16]. The corresponding solver diagram is shown in Figure 4. All operator evaluations are performed using the matrix-free infrastructure described in [22, 23] to ensure a high node-level performance, following the current trends of exascale finite-element algorithms described in [21]. Hence, we embed the IRK methods in a—with regard to communication costs—challenging context where differences are most pronounced.

All experiments are conducted on the SuperMUC-NG supercomputer. Its compute nodes have 2 sockets (each with 24 cores of Intel Xeon Skylake) and the AVX-512 ISA extension so that 8 doubles can be processed per instruction.³ As compiler, we use `g++` (version 9.1.0) with the flags `-O3 -funroll-loops -march=skylake-avx512`.

5.1 Moderately parallel runs

We start with the analysis of the performance of the proposed stage-parallel algorithm at small scales with 786 processes (16 compute nodes) as an example. Figure 5 shows the runtime per time step and the throughput for stage-parallel IRK and IRK for $k=1$ and $Q=4$. Furthermore, we present data for IRK with 192 ($=786/4$) processes, to which we compare the obtained speedup. For large problem sizes, IRK with four times the number of processes achieves a speedup of 3.7. However, its performance quickly drops for smaller sizes and times comparable to the 192-process case are reached. In this range, the number of processes used does not influence the times and inherently serial parts of the code (like latency of communication and the coarse-grid solver) dominate. In the case of stage-parallel IRK, we see a different behavior: over large refinement ranges,

³<https://doku.lrz.de/display/PUBLIC/SuperMUC-NG>, retrieved on February 26, 2022.

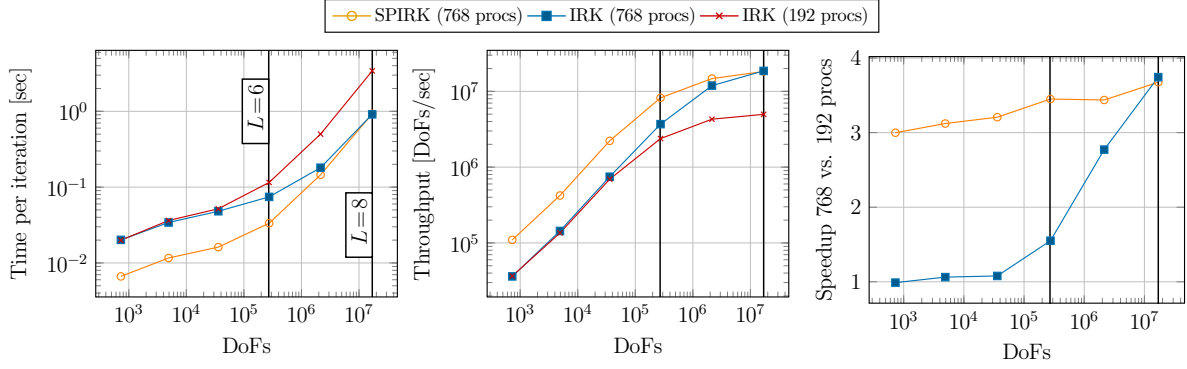


Figure 5: Comparison of stage-parallel IRK with 768 processes, of IRK with 768 processes, and of IRK with 192(=768/4) processes for $Q=4$ and $k=1$: time and throughput per time step as well as speedup.

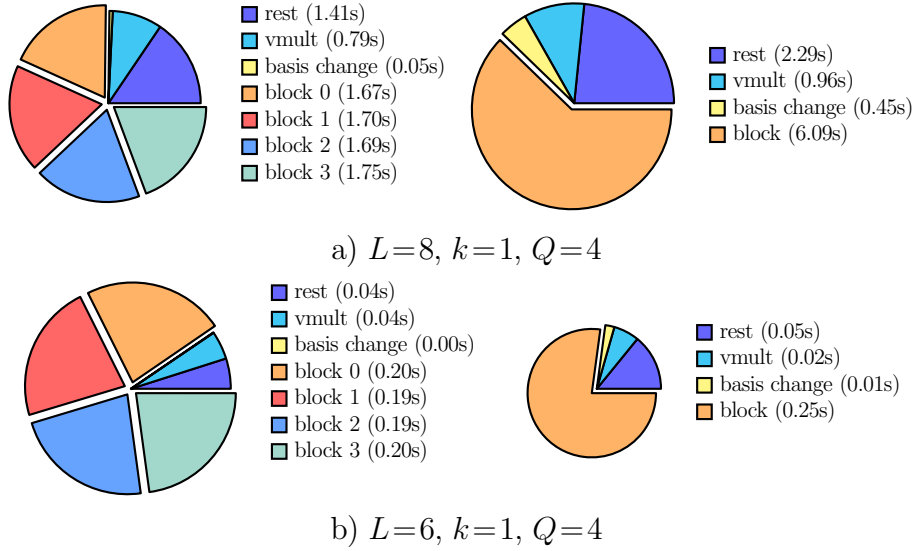


Figure 6: Time spent for matrix-vector product (vmult), basis change, block solvers, and the remaining operations (setup of right-hand-side vector of (1), vector updates, etc.) for IRK (left) and stage-parallel IRK (right). The area of the circles indicates the total time compared to the other version.

a speedup of >3 can be reached. The maximum value is lower than in the IRK case ($3.6 < 3.7$).

Figure 6 presents—in accordance with the traces in Figure 3—pie diagrams visualizing the time spent on different parts of the algorithms. In particular, they show the time for basis change S/S^{-1} and for the solution of each block or of the whole preconditioner in the case of IRK or of stage-parallel IRK, correspondingly. The pie diagrams are provided for two refinement configurations: $L=8$ (far away from the scaling limit) and $L=6$ (close to the scaling limit). Starting with $L=8$, one can see that, in the case of IRK, the block preconditioners are dominating in the total time (75%) and the basis changes are negligible (1%). In the case of stage-parallel IRK, one can see that the time spent on the (single) preconditioner application has decreased, but the times for setting up the right-hand-side vector, the matrix-vector product, and the basis changes during preconditioning have slightly increased. This is not surprising, since these are operations where communication between stages is required and processes are implicitly synchronized by

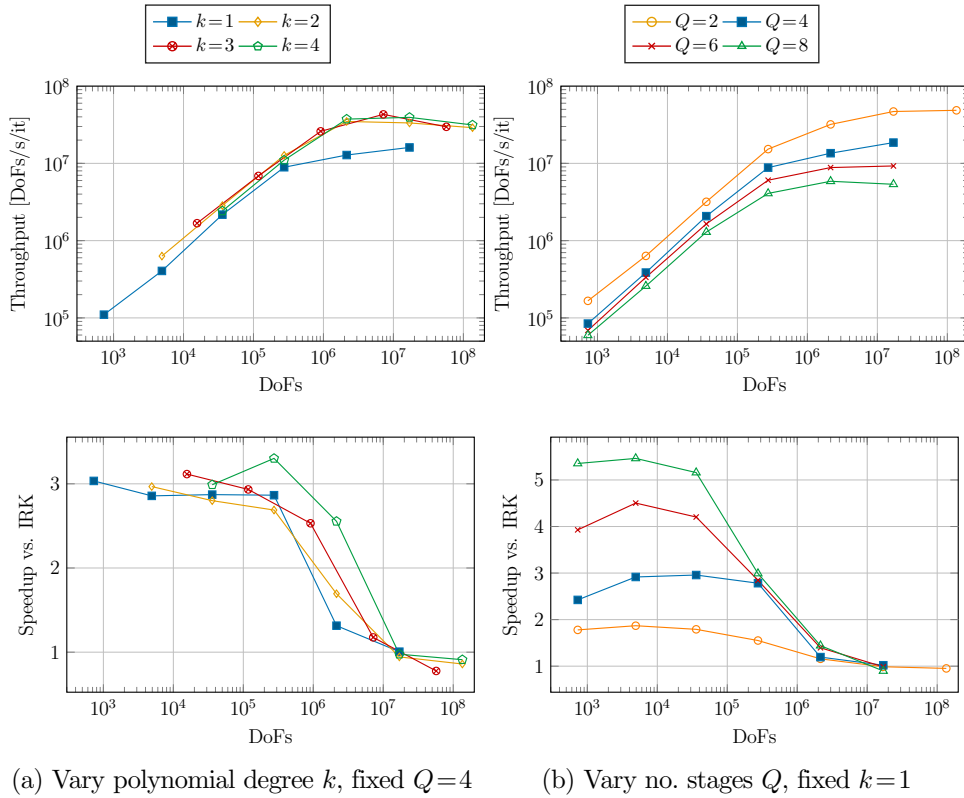


Figure 7: Influence of parameters on the performance of stage-parallel IRK and the speedup of stage-parallel IRK as compared to IRK on 16 nodes / 768 MPI processes.

the rotation of the vectors. For $L=6$, the ratio of preconditioning becomes an even more dominating part of the total solution time (90%/77%). However, one can see that the total time spent for preconditioning reduces by a factor of 3.1 in the case of stage-parallel IRK compared to IRK.

Influence of key parameters

Figure 7 shows the influence of the parameters “polynomial degree k ” and “number of stages Q ” on the performance and speedup of stage-parallel IRK compared to IRK with the same number of processes. The following observations can be made.

Large polynomial degrees k increase the throughput of matrix-free operator evaluation. As a consequence, the throughput of IRK also rises with increasing polynomial degree, since its most time-consuming component—the geometric-multigrid solver—is also implemented in a matrix-free way. Furthermore, increasing k seems to also have a positive effect on the speedup of stage-parallel IRK.

The number of stages Q has the most significant influence on the throughput of IRK and stage-parallel IRK. This is not surprising, since the work per time step increases with the number of stages. However, the observed drop in throughput is more significant than expected from the increase in work alone. This is explained by the number of outer iterations, which increases slightly with the number of stages. The achievable speedup with stage-parallel IRK rises with increasing number of stages. In addition, Table 2 shows the average number of

Table 2: Comparison of number of GMRES iterations ($\#G$) and of accumulated V-cycle applications ($\#V$) per time step for non-complex/complex IRK and stage-parallel IRK. For the stage-parallel IRK, the reported numbers of iterations and cycles are shown for process groups. Since complex stage-parallel IRK runs GMRES independently on the blocks, the number of GMRES iterations and, consequently, the number of V-cycle applications vary between blocks. In this case, we report the minimum and maximum values. Numbers are shown for different Q and $k=1$, $L=8$. The additional superscript of $\#V$ specifies the number of blocks a GMG V-cycle considers.

non-complex (Sections 2-5)				
	IRK	SPIRK	batched	
Q	$\#G$ ($\#V^1$)	$\#G$ ($\#V^1$)	$\#G$ ($\#V^Q$)	
2	5.0 (12.0)	5.0 (6.0)	5.0 (6.0)	
4	7.0 (32.0)	7.0 (8.0)	7.8 (8.8)	
6	9.9 (65.3)	9.9 (10.9)	9.9 (10.9)	
8	11.9 (103.1)	11.9 (12.9)	11.0 (12.0)	

complex (Section 6)				
	IRK-PRESB	IRK-GMG	SPIRK-PRESB	SPIRK-GMG
Q	$\#G$ ($\#V^1$)	$\#G$ ($\#V^2$)	$\#G$ ($\#V^1$)	$\#G$ ($\#V^2$)
2	6.0 (14.0)	7.0 (8.0)	6.0 (14.0)	7.0 (8.0)
4	11.6 (27.1)	14.0 (16.0)	5.6-6.0 (13.1-14.0)	7.0-7.0 (8.0-8.0)
6	18.2 (42.4)	22.0 (25.0)	6.0-6.2 (14.0-14.4)	7.0-8.0 (8.0-9.0)
8	23.1 (54.2)	31.3 (35.3)	5.0-6.1 (12.0-14.2)	7.0-9.3 (8.0-10.3)

GMRES iterations and accumulated numbers of V-cycles that are run in parallel. One can see, on the one hand, that the number of GMRES iterations increase from 5 to 12 when going from $Q=2$ to $Q=8$ and, on the other hand, that stage-parallel execution allows to reduce, e.g., for $Q=8$, the number of V-cycles run sequentially by a factor of 8 from 103 to 12, matching the measured timings and speedups in Figure 7.

Making definite general conclusions is not straightforward as they depend on the number of processes, the type of the coarse mesh, the refinement, the partial differential equation, and the block solvers. However, we believe that similar trends can be observed in different setups. We should note however, that we use the heat equation as a test problem, for which we have efficient and well-scaling block preconditioners based on multigrid methods. For other classes of problems where optimally scaling block solvers are more challenging to design, we would expect to observe differences between stage-parallel IRK and IRK also for smaller problem sizes. In the worst case, when the blocks are solved by direct methods, stage parallelism might be the only way to parallelize the work. However, there is evidence for advantages of more advanced solvers, such as the block Jacobi solver with local ILU as considered by [28].

5.2 Virtual topology and shared memory

In Section 3.1, we presented a row-major lexicographical enumeration of processes. This enumeration favors the operation $\mathbf{v} = (D \otimes \mathbb{I}_n) \mathbf{u}$, since the data needed are in close proximity and maybe even on the same compute node. However, it is not optimal for the inner (multigrid) solver, for which a column-major enumeration (Figure 8c), placing nearby spatial partitions on the same node, would be favorable. In the following, we compare these two virtual topologies.

Furthermore, we investigate the benefits of using shared-memory features of MPI during $\mathbf{v} = (D \otimes \mathbb{I}_n) \mathbf{u}$. For this, a modified row-major enumeration is beneficial. We introduce a



Figure 8: Different virtual topologies to increase data locality a) for the basis change S and c) for the inner preconditioner. Version b) introduces padding to guarantee that all stages are on the same shared-memory domain/same compute node.

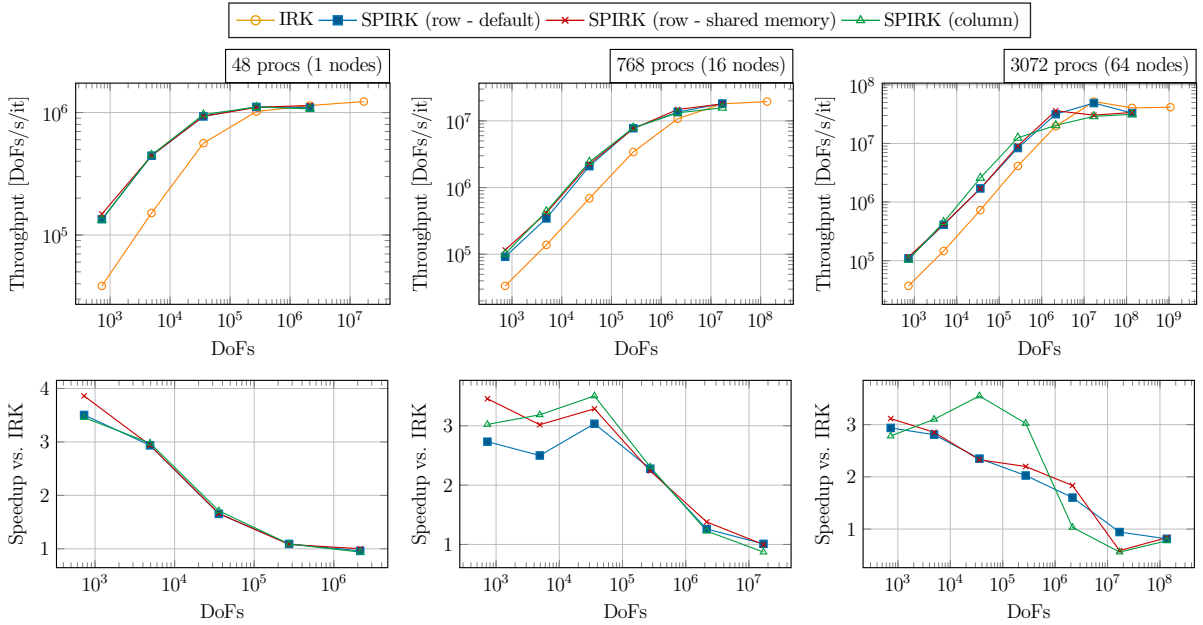


Figure 9: Comparison of virtual topologies for $k=1$ and $Q=4$.

padding—as indicated in Figure 8b)—in such a way that all processes of a stage are assigned to the same compute node similarly as also done in [28]. This allows us to skip the communication of complete vectors as their entries can be accessed directly. In order to prevent race conditions, we introduce barriers across the processes in `comm_row`, which are equivalent to the implicit barriers in the case of parallel for loops in `OpenMP`.

Figure 9 shows the experimental results for $k=1$ and $Q=4$ on 1, 16, and 64 compute nodes. Generally, the different virtual topologies show similar behaviors. Using shared memory leads to a speedup in a few cases, but overall the improvement is not significant in terms of performance. This is because the basis change is not the bottleneck, as discussed in the previous sections. Overall, the column-major enumeration seems to give the best results in the intermediate regime. However, it also turns out to be the slowest virtual topology far from the scaling limit, indicating

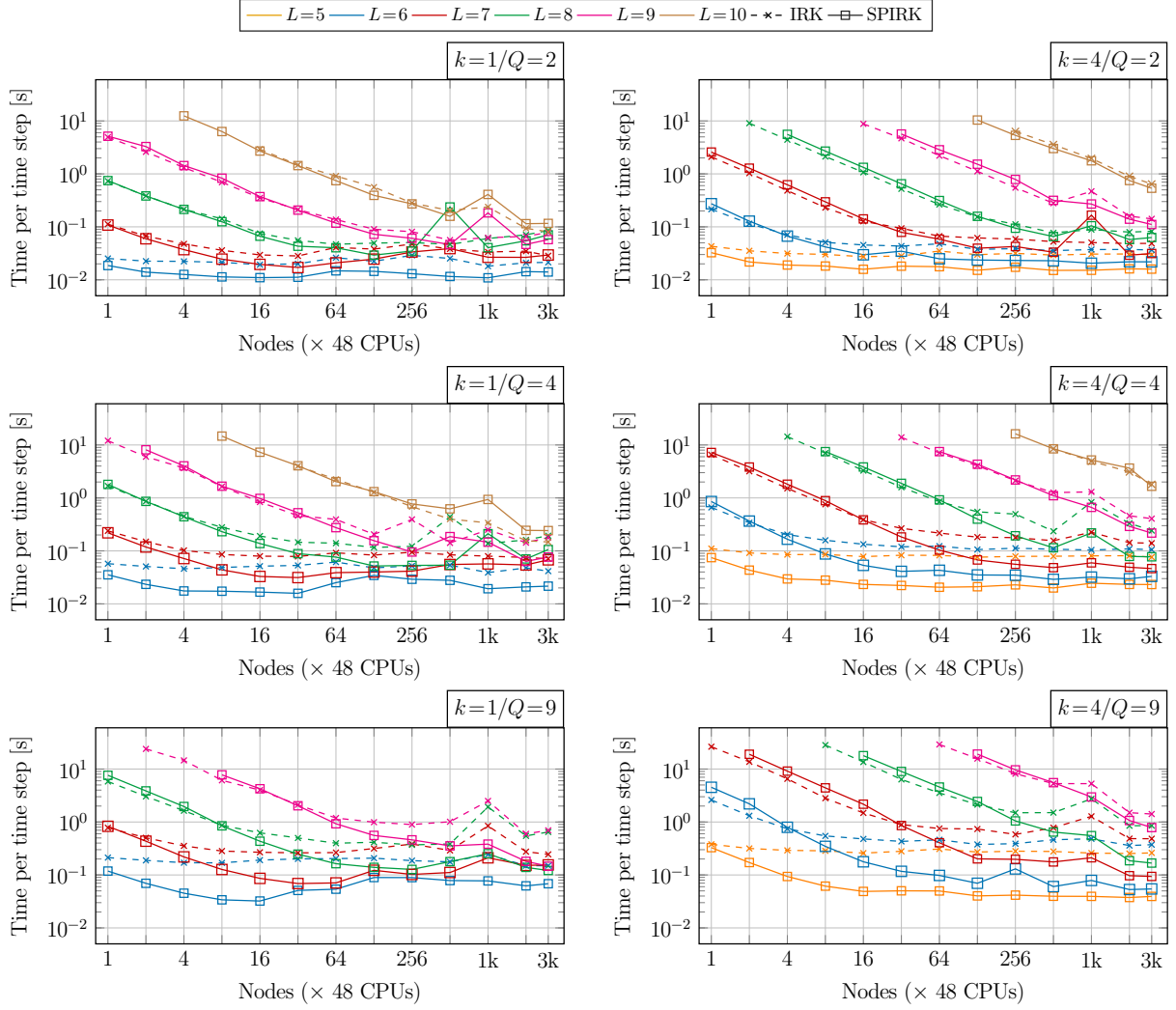


Figure 10: Strong-scaling comparison (time per time step) of IRK and stage-parallel IRK for $k=1/k=4$ and $Q=2/Q=4/Q=9$.

that the increased costs of the basis change cannot be counterbalanced by the faster block solver.

5.3 Large-scale parallel runs

Figure 10 shows the results of scaling experiments starting with 1 compute node (48 processes) up to 3,072 nodes (147,456 processes) for different polynomial degrees ($k=1/k=4$) and numbers of stages ($Q=2/Q=4/Q=9$). One can clearly see that stage-parallel IRK reaches lower times to solution at the scaling limit. Figure 11 and 12 give more insights, by providing normalized plots (throughput of one time step/per stage) of the same results of all considered values of Q in a single diagram. Far from the scaling limit (right top corner of the plots), IRK tends to be more efficient. Stage-parallel IRK, on the contrary, reaches lower times per time step at the scaling limit (left bottom corner of the plots) at the cost of lower efficiencies. Furthermore, the diagrams allow to compare the effect of the value of Q , as is similarly done in Subsection 5.1 for moderate number of processes. Here, one can again see that the costs are increasing with the number of stages, particularly also due to the increasing number of outer iterations, which

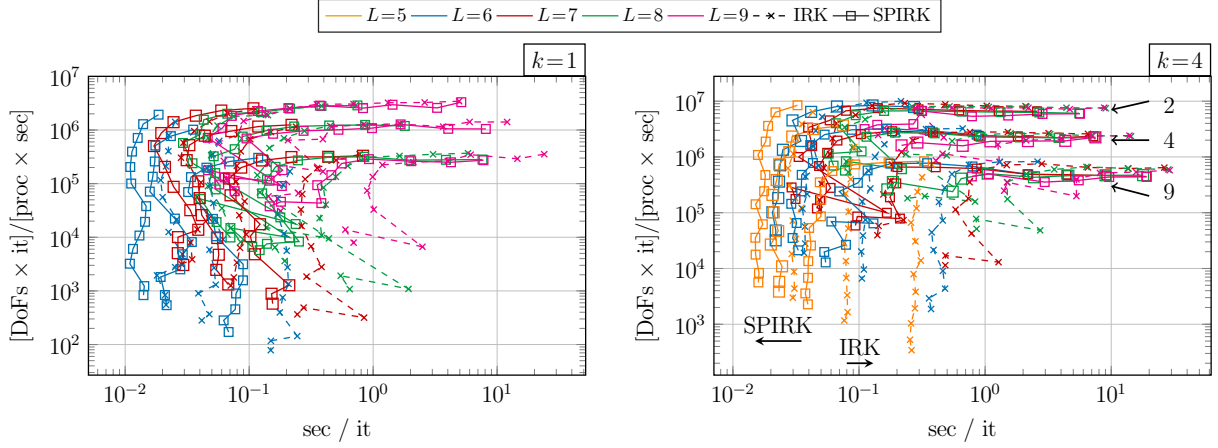


Figure 11: Strong scaling: throughput of a time step (results from Figure 10).

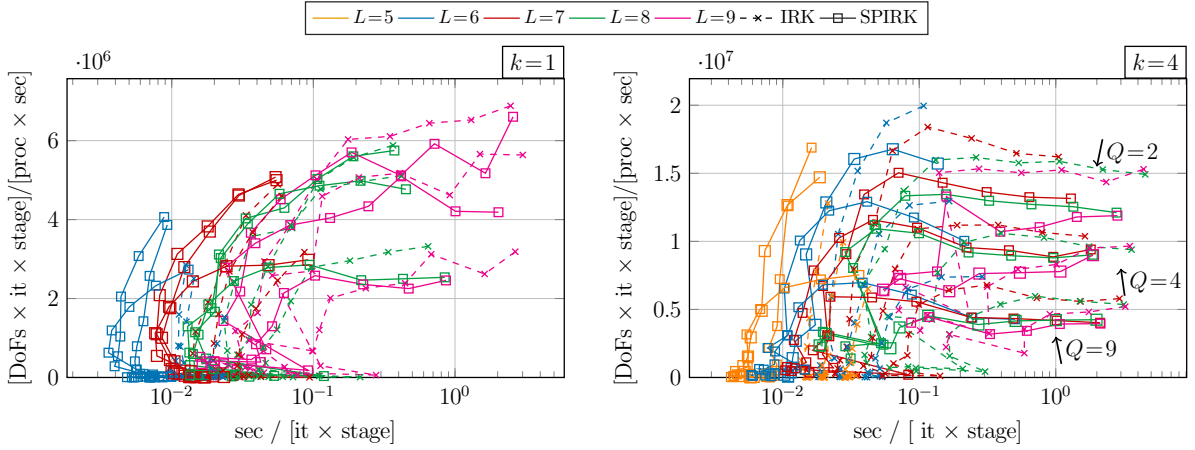


Figure 12: Strong scaling: throughput per stage (results from Figure 10)

influences the scaling limits as well. However, we recall that a high number of stages allows to use bigger time steps due to an increased accuracy so that the additional costs might amortize.

As a summary, Figure 13 shows the measured speedup of stage-parallel IRK in comparison to IRK, categorized according to the number of DoFs per process. A clear speedup is obtained for less than 10k DoFs per process, i.e., half a million DoFs per node. For larger problem sizes per process, the picture is split. For more than 100k DoFs per process, IRK is consistently faster ($\approx 20\%$).

5.4 Batched execution

For the batched experiments, we replace the coarse-grid solver AMG by Chebyshev iterations around a point-Jacobi method with the same settings as of the smoothers (cf. Section 5). Furthermore, we do not set up the coefficients of the Chebyshev polynomials for each block separately, but instead set them up with the approximation of the maximum eigenvalue of all blocks. This choice does not negatively affect the number of GMRES iterations, as indicated by Table 2.

Figure 14a) shows the timings of a batched execution of IRK on 16 nodes. The results are somewhat disappointing compared to our performance model and the number of iterations

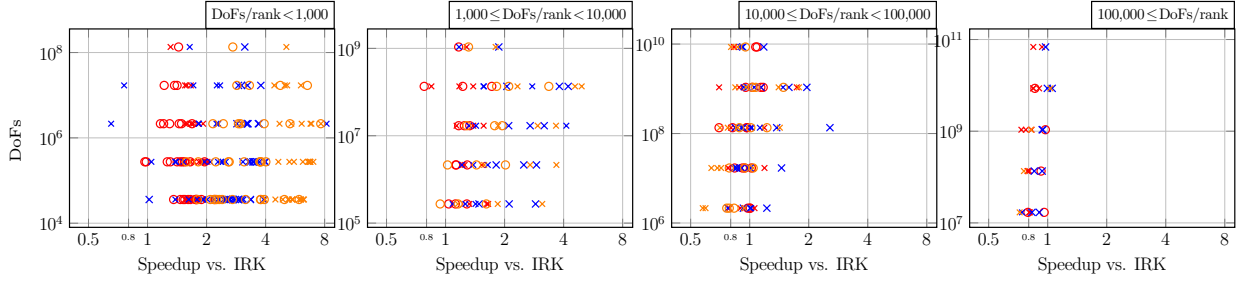


Figure 13: Strong scaling: speedup categorized according to number of DoFs per process (results from Figure 10). Circles/x indicate $k=1/k=4$ and the colors red/blue/orange indicate $Q=2/Q=4/Q=9$.

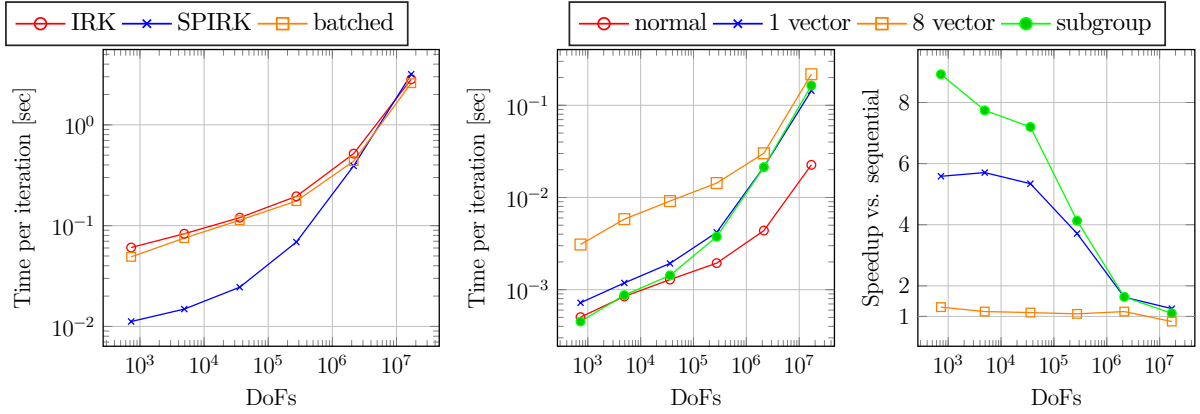


Figure 14: a) Comparison of time per iteration of IRK, stage-parallel IRK, and batch IRK for $k=1$ and $Q=8$ with 768 processes (16 compute nodes); b-c) time of iteration and speedup of different execution modes to process $Q=8$ stages in comparison to a sequential execution of the stages.

documented in Table 2. The timings are similar to the serial execution and only small speedup are obtained, e.g., for $Q=8$, 5–25%.

The cause for this behavior is that the communication during the intergrid transfer in deal.II is serialized for each stage. This is due to a design choice of allowing black-box processing of the stages with a separate vector for each stage. By collecting all stages in a single vector, this issue could be overcome, as indicated by preliminary results obtained for GMG. Figures 14b-c) show timings and speedup of a single-vector execution, of an execution with Q vectors, and of an execution with Q subgroups, in comparison to a sequential execution.

The results highlight the importance of batching all parts of the code. If this is not possible for all identified code paths, the execution gets serialized and scalability is limited. The results for GMG indicate that one can expect higher speedups (up to 5.7 for $Q=8$) for batched execution; however, the speedup will be probably smaller than in the case of the execution on subgroups.

We point out that using non-Cartesian meshes might shift the benefit from grouped execution towards a batched one, since loading Jacobian matrices per quadrature point only once and not Q times (once per process group) might be beneficial, as discussed in Section 3.4.

6 Real vs. complex arithmetic – a comparison

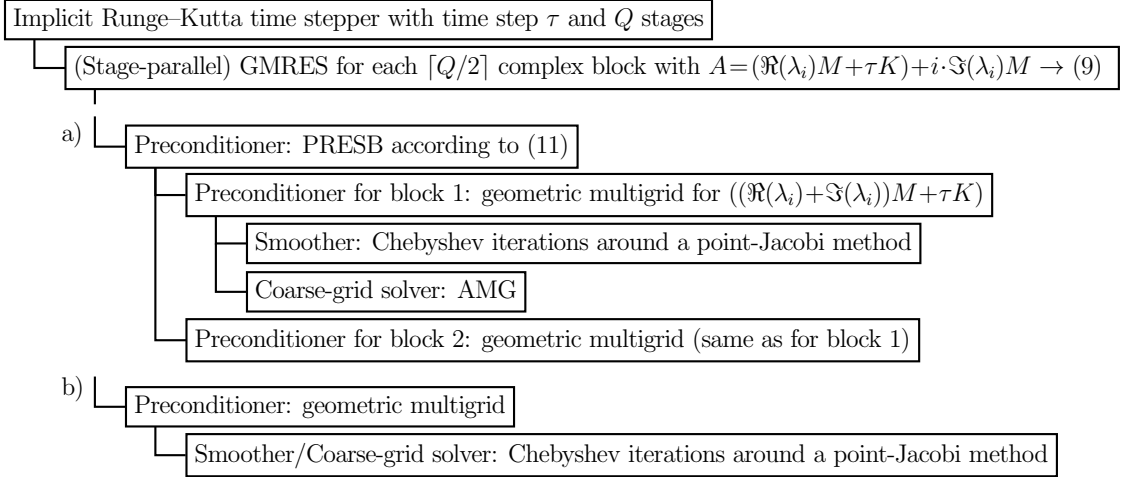


Figure 15: Diagram of the complex solvers used to solve the heat problem in Section 6: a) PRESB as preconditioner, b) GMG as preconditioner.

For the IRK algorithm described in Section 2, we have chosen L as basis of the preconditioner, since its eigenvalues and eigenvectors are real and the resulting block system to be solved is real as well. However, the proposed concepts regarding stage-parallel implementation—particularly the data distribution and the communication patterns—are also applicable to the complex case, which arises when A_Q^{-1} is diagonalized directly. The advantage of factorizing A_Q^{-1} directly is that no global GMRES iterations—consisting of all Q stages—are needed and one can solve each block individually after the basis change. However, the disadvantage is that each block in (2) is complex:

$$\lambda_i M + \tau K = (\Re(\lambda_i) + i \cdot \Im(\lambda_i))M + \tau K = \underbrace{(\Re(\lambda_i)M + \tau K)}_{K'_i} + i \cdot \underbrace{\Im(\lambda_i)M}_{M'_i}, \quad (9)$$

with $\lambda_i = \Re(\lambda_i) + i \cdot \Im(\lambda_i)$. Written as a two-by-two block-matrix system, $(K'_i + iM'_i)\mathbf{u}_i = \mathbf{v}_i$ becomes:

$$\begin{bmatrix} K'_i & -M'_i \\ M'_i & K_i \end{bmatrix} \begin{bmatrix} \Re(\mathbf{u}_i) \\ \Im(\mathbf{u}_i) \end{bmatrix} = \begin{bmatrix} \Re(\mathbf{v}_i) \\ \Im(\mathbf{v}_i) \end{bmatrix}. \quad (10)$$

Since the structure of the resulting system is similar to that of a real Schur complement and, therefore, the algorithms to solve the system are equivalent, we will not detail this approach.

For systems of the type (10), PRESB is an efficient preconditioner [8]:

$$P_i = \begin{bmatrix} K'_i & -M'_i \\ M'_i & K_i + 2M'_i \end{bmatrix} = \begin{bmatrix} I & -I \\ 0 & I \end{bmatrix} \begin{bmatrix} K'_i + M'_i & 0 \\ M'_i & K'_i + M'_i \end{bmatrix} \begin{bmatrix} I & I \\ 0 & I \end{bmatrix} \quad (11)$$

For approximating the inverse of $(K'_i + M'_i)$, we use a single V-cycle. The corresponding solver diagram is shown in Figure 15a). Please note that the blocks corresponding to the real and imaginary part have to be solved in sequence (2 V-cycles), possibly limiting the scalability.

Alternatively to PRESB, we also consider GMG applied directly to (10), consisting of both real and imaginary blocks. The corresponding solver diagram is shown in Figure 15b). The motivation for this is similar to the one of batched IRK: at the scaling limit, running one

V-cycle on a vector with twice as many DoFs might be cheaper than running 2 V-cycles on smaller vectors in sequence.

The block structure of the transformed system (2) has some influence on the algorithms presented in Section 3. The fact that only $\lceil Q/2 \rceil$ blocks can be solved independently allows to parallelize only between $\lceil Q/2 \rceil$ “stages”. Naturally, each process group would be responsible for a stage pair. Furthermore, operations of the form $\mathbf{v} = (D \otimes \mathbb{I}_n) \mathbf{u}$ need minor adjustments, depending on the usage:

- application of A_Q^{-1} ($\mathbf{u}, \mathbf{v} \in \mathbb{R}^{n \times Q}$, $D \in \mathbb{R}^{Q \times Q}$) with stages assigned to $\lceil Q/2 \rceil$ processes and
- application of S^{-1} ($\mathbf{u} \in \mathbb{R}^{n \times Q}$, $\mathbf{v} \in \mathbb{C}^{n \times \lceil Q/2 \rceil}$, $D \in \mathbb{C}^{\lceil Q/2 \rceil \times Q}$) and of S ($\mathbf{u} \in \mathbb{C}^{n \times \lceil Q/2 \rceil}$, $\mathbf{v} \in \mathbb{R}^{n \times Q}$, $D \in \mathbb{C}^{Q \times \lceil Q/2 \rceil}$).

In these cases, the distributed tensor algorithms from Section 3 can be extended. They work on blocks of two vectors and perform block operations between the rotation steps, e.g.,

$$\begin{bmatrix} \mathbf{v}_1 \\ \mathbf{v}_2 \\ \vdots \end{bmatrix} = \begin{bmatrix} D_{11} \mathbf{u}_1 + D_{12} \mathbf{u}_2 \\ D_{21} \mathbf{u}_1 + D_{22} \mathbf{u}_2 \\ \vdots \end{bmatrix} + \begin{bmatrix} D_{13} \mathbf{u}_3 + D_{14} \mathbf{u}_4 \\ D_{23} \mathbf{u}_3 + D_{24} \mathbf{u}_4 \\ \vdots \end{bmatrix} + \dots$$

as block extension of (6).

The performance models derived in Section 4 are also applicable to the complex case, with more pressure on the block solvers/preconditioners. The basis change—resulting in an implicit synchronization between all stages—has to be performed only once per time step, since the $\lceil Q/2 \rceil$ blocks can be solved independently. Each block solve might be more expensive, since they might involve the solution of a two-by-two system. Comparing the complex case with the approximate case in real arithmetic, it is obvious that we lose some possibilities for (stage) parallelization by the reduction of the number of blocks ($Q \rightarrow \lceil Q/2 \rceil$) and by the sequential execution of two GMG V-cycles in the PRESB case. Not surprisingly, the obtained speedup (Figure 16) is about half of the one of the stage-parallel preconditioner, which allows the parallel execution of all stages (see Figure 7). However, only two basis changes need to be performed per time step, which reduces the number of possibly expensive synchronization points.

According to our performance model, the total execution time at the scaling limit will be dominated by the maximum number of accumulated GMG iterations each process group has to execute. Hence, non-complex stage-parallel IRK might be advantageous for low values of Q , but complex stage-parallel IRK might be competitive for high Q , since the number of iterations per stage is independent of Q . The results in Figure 17 verify our expectations, by comparing the times of the real-valued IRK studied before against the complex-valued IRK and the stage-parallel IRK solvers. Surprisingly, the two stage-parallel IRK algorithms show similar times for small problem sizes, demonstrating that the growing iteration counts of the outer solver of the non-complex solver—indicated by the growing gap between the IRK implementations—can be compensated by its better parallel behavior. This can also be seen in Table 2, which shows a similar number of V-cycles to be executed in the context of non-complex and complex stage-parallel IRK, respectively. However, we would like to note that it is hard to make a fair comparison, since the tolerances have different meanings in the complex and the non-complex case. Furthermore, it was easy to integrate efficient complex arithmetic in our small benchmarks, but this might not be the case when the time steppers should be applied

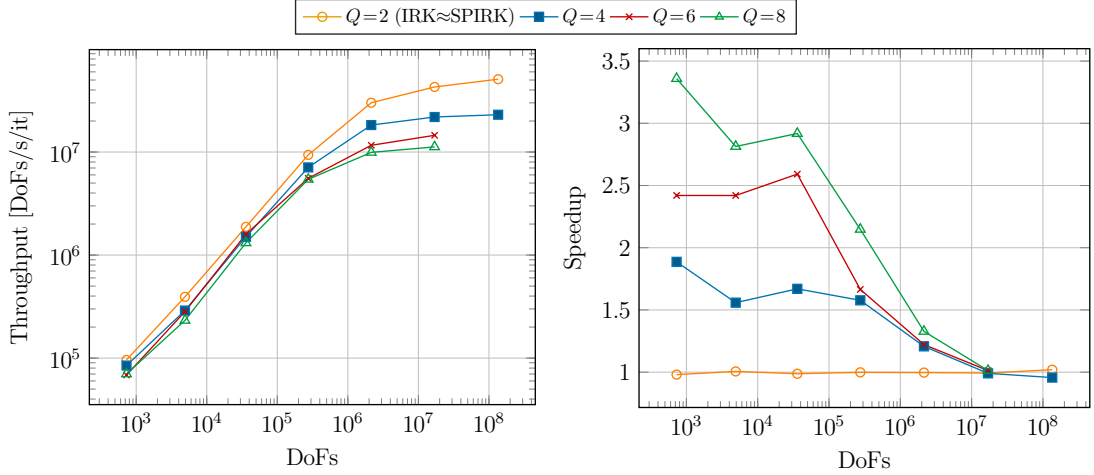


Figure 16: Throughput and speedup of complex stage-parallel IRK vs. complex IRK with PRESB for $k=1$ with 768 processes (16 compute nodes).

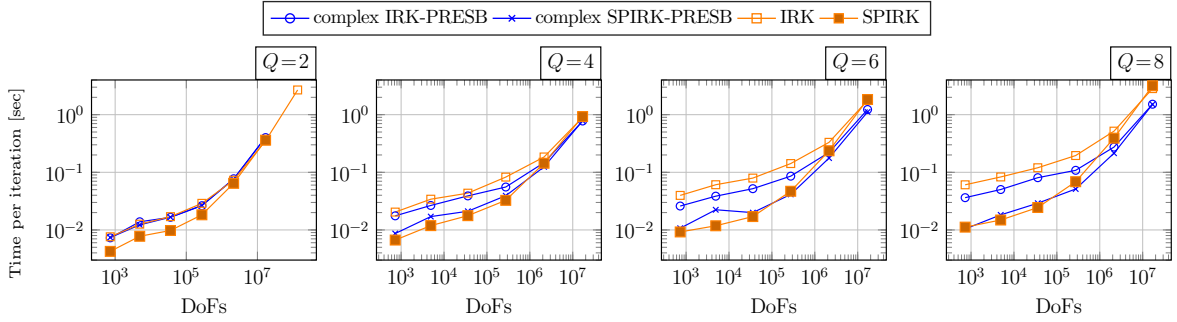


Figure 17: Comparison of throughputs of non-complex/complex IRK and stage-parallel IRK for $k=1$ with 768 processes (16 compute nodes).

in a black-box fashion. Against this background, a more detailed analysis for when to favor one method over the other is subject of future work.

Figure 18 compares the solution times of PRESB and GMG as preconditioners. Overall, PRESB seems to be superior compared to GMG due to fewer GMRES iterations (see Table 2). However, the scalability is comparable. In fact, Table 2 shows that GMG needs less V-cycles in total, indicating potential for better scalability of GMG once the optimizations discussed in Section 5.4 have been realized.

Recently, Southworth et al. [30] presented a novel solver for IRK. They also exploit the complex-conjugate property of the eigenvalues and solve the pairs together. For preconditioning the blocks, they apply 2 V-cycles of (algebraic) multigrid as well. However, it is a bit more involved to solve the blocks, since they have the form $(\Re(\lambda_i)\mathbb{I}_n - \delta t M^{-1}K)^2 + \Im(\lambda_i)\mathbb{I}_n$. The algorithm proposed in that study is, however, inherently stage-serial as it requires the sequential solution of stage (pairs) by construction so that the algorithms presented in our publication are not applicable there.

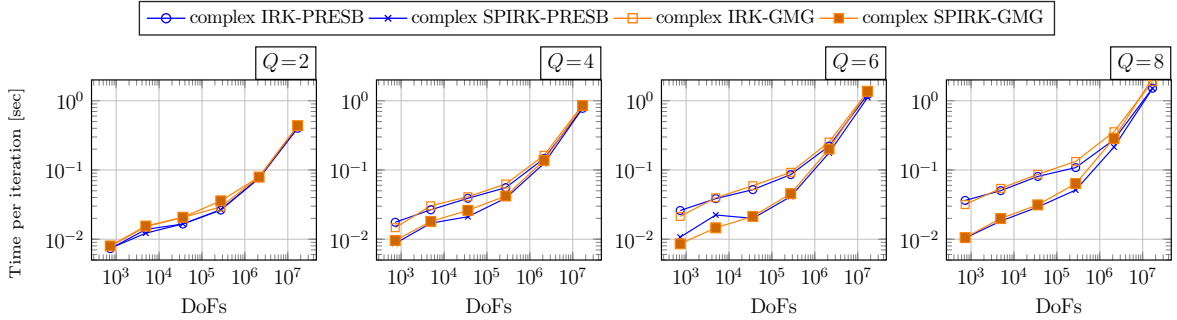


Figure 18: Comparison of throughputs of complex IRK and stage-parallel IRK with PRESB or GMG as preconditioner for $k=1$ with 768 processes (16 compute nodes).

7 Conclusions & outlook

For distributed memory computing platforms, we have presented implementations of implicit Runge–Kutta algorithms, including the novel preconditioner proposed in Axelsson and Neytcheva [7]. The algorithms allow to run the matrix-vector multiplication and preconditioner in parallel by process groups associated with each stage. Upon a basis change—involving all stages—inner block solvers can be applied independently in a black-box fashion. We have identified that the tensor operations $\mathbf{v} = (\mathbb{I}_Q \otimes C)\mathbf{u}$ and $\mathbf{v} = (D \otimes \mathbb{I}_n)\mathbf{u}$ are the main building blocks, and have proposed efficient parallel algorithms.

We have presented a detailed performance analysis of the stage-parallel preconditioner implementation for a time-dependent heat problem on up to 150k processes on 3k CPU compute nodes, using state-of-the-art matrix-free geometric multigrid solvers. Furthermore, we have compared its performance to the one of an implementation not using stage parallelism. We observed that the stage-parallel implementation is able to significantly shift the scaling limit and reaches speedups $\leq Q$. In absolute numbers, the proposed solvers and implementations make it possible to obtain high solver efficiencies down to less than 0.05 seconds per time step for four-stage IRK schemes. However, far from the scaling limit, possible load imbalances between the solvers of the stages and communication overhead lead to a slight drop in performance in comparison to the non-stage-parallel IRK implementation with 13% lower throughput on average.

The algorithms are also applicable to the case when the system matrix arising from implicit Runge–Kutta method is directly factorized, requiring complex arithmetic or the solution of two-by-two blocks. This limits the scalability in comparison to the case of the stage-parallel preconditioner. Results, however, show that the lower number of iterations and the scalability balance each other, leading to similar minimum times to solution of stage-parallel direct factorization and preconditioning for a high number of stages ($Q \leq 8$).

We have also discussed batching the operations of all stages instead of assigning each stage to a process group, showing the challenge in terms of black-box interfaces. In future work, we plan to study stage parallelism for non-linear partial differential equations, e.g., Navier–Stokes equations. Furthermore, we intend to improve the batched implementation as well as make further investigations of its performance and usability within a library context, which might require code generation [15].

Acknowledgments

The authors acknowledge collaboration with the `deal.II` community. This work was supported by the Bayerisches Kompetenznetzwerk für Technisch-Wissenschaftliches Hoch- und Höchstleistungsrechnen (KONWIHR) through the project “High-order matrix-free finite element implementations with hybrid parallelization and improved data locality”. The authors gratefully acknowledge the Gauss Centre for Supercomputing e.V. (www.gauss-centre.eu) for funding this project by providing computing time on the GCS Supercomputer SuperMUC-NG at Leibniz Supercomputing Centre (LRZ, www.lrz.de) through project id pr83te.

References

- [1] R. ABU-LABDEH, S. MACLACHLAN, AND P. E. FARRELL, *Monolithic multigrid for implicit Runge–Kutta discretizations of incompressible fluid flow*, arXiv preprint arXiv:2202.07381, (2022).
- [2] M. ADAMS, M. BREZINA, J. HU, AND R. TUMINARO, *Parallel multigrid smoothing: polynomial versus Gauss–Seidel*, *Journal of Computational Physics*, 188 (2003), pp. 593–610.
- [3] D. ARNDT, W. BANGERTH, B. BLAIS, M. FEHLING, R. GASSMÖLLER, T. HEISTER, L. HELTAI, U. KÖCHER, M. KRONBICHLER, M. MAIER, P. MUNCH, J.-P. PELTERET, S. PROELL, K. SIMON, B. TURCK SIN, D. WELLS, AND J. ZHANG, *The deal.II library, version 9.3*, *Journal of Numerical Mathematics*, 29 (2021), pp. 171–186.
- [4] D. ARNDT, W. BANGERTH, D. DAVYDOV, T. HEISTER, L. HELTAI, M. KRONBICHLER, M. MAIER, J.-P. PELTERET, B. TURCK SIN, AND D. WELLS, *The deal.II finite element library: Design, features, and insights*, *Computers & Mathematics with Applications*, 81 (2021), pp. 407–422.
- [5] O. AXELSSON, *Global integration of differential equations through Lobatto quadrature*, *BIT – Nordisk Tidskrift for Informationsbehandling*, 4 (1964), pp. 69–86.
- [6] O. AXELSSON, I. DRAVINS, AND M. NEYTCHEVA, *Stage-parallel preconditioners for implicit Runge-Kutta methods of arbitrary high order. Linear problems*, Uppsala University. Technical reports from the Department of Information Technology 2022-004, (2022).
- [7] O. AXELSSON AND M. NEYTCHEVA, *Numerical solution methods for implicit runge-kutta methods of arbitrarily high order*, in 21st Conference on Scientific Computing, Vysoké Tatry-Podbanské, Slovakia, September 10-15, 2020, vol. 7, 2020, pp. 11–20.
- [8] O. AXELSSON, M. POURBAGHER, AND D. K. SALKUYEH, *Robust iteration methods for complex systems with an indefinite matrix term*, arXiv preprint arXiv:2110.00537, (2021).
- [9] T. A. BICKART, *An efficient solution process for implicit Runge–Kutta methods*, *SIAM Journal on Numerical Analysis*, 14 (1977), pp. 1022–1027.
- [10] M. BOLTEN, D. MOSER, AND R. SPECH, *A multigrid perspective on the parallel full approximation scheme in space and time*, *Numerical Linear Algebra with Applications*, 24 (2017), p. e2110.

- [11] K. BURRAGE, C. ELDERSHAW, AND R. SIDJE, *A parallel matrix-free implementation of a Runge–Kutta code*, in Joint Australian-Taiwanese Workshop on Analysis and Applications, Australian National University, Mathematical Sciences Institute, 1999, pp. 83–88.
- [12] J. C. BUTCHER, *On the implementation of implicit Runge–Kutta methods*, BIT Numerical Mathematics, 16 (1976), pp. 237–240.
- [13] L. E. CANNON, *A cellular computer to implement the Kalman filter algorithm*, Montana State University, 1969.
- [14] J. J. B. DE SWART, W. M. LIOEN, AND W. A. VAN DER VEEN, *Specification of PSIDE*, Citeseer, 1998.
- [15] P. E. FARRELL, R. C. KIRBY, AND J. MARCHENA-MENENDEZ, *Irksome: Automating Runge–Kutta time-stepping for finite element methods*, ACM Transactions on Mathematical Software (TOMS), 47 (2021), pp. 1–26.
- [16] M. W. GEE, C. M. SIEFERT, J. J. HU, R. S. TUMINARO, AND M. G. SALA, *ML 5.0 smoothed aggregation user’s guide*, tech. report, Technical Report SAND2006-2649, Sandia National Laboratories, 2006.
- [17] G. HAGER AND G. WELLEIN, *Introduction to high performance computing for scientists and engineers*, CRC Press, 2010.
- [18] K. R. JACKSON AND S. P. NØRSETT, *The potential for parallelism in Runge–Kutta methods. Part I. RK formulas in standard form*, Journal on Numerical Analysis, 32 (1995), pp. 49–82.
- [19] L. O. JAY AND T. BRACONNIER, *A parallelizable preconditioner for the iterative solution of implicit Runge–Kutta-type methods*, Journal of computational and applied mathematics, 111 (1999), pp. 63–76.
- [20] C. A. KENNEDY, M. H. CARPENTER, AND R. M. LEWIS, *Low-storage, explicit Runge–Kutta schemes for the compressible Navier–Stokes equations*, Applied Numerical Mathematics, 35 (2000), pp. 177–219.
- [21] T. KOLEV, P. FISCHER, M. MIN, J. DONGARRA, J. BROWN, V. DOBREV, T. WARBURTON, S. TOMOV, M. S. SHEPHARD, A. ABDELFAH, V. BARRA, N. BEAMS, J.-S. CAMIER, N. CHALMERS, Y. DUDOUIT, A. KARAKUS, I. KARLIN, S. KERKEMEIER, Y.-H. LAN, D. MEDINA, E. MERZARI, A. OBABKO, W. PAZNER, T. RATHNAYAKE, C. W. SMITH, L. SPIES, K. SWIRYDOWICZ, J. THOMPSON, A. TOMBOULIDES, AND V. TOMOV, *Efficient exascale discretizations: High-order finite element methods*, The International Journal of High Performance Computing Applications, 35 (2021), pp. 527–552.
- [22] M. KRONBICHLER AND K. KORMANN, *A generic interface for parallel cell-based finite element operator application*, Computers & Fluids, 63 (2012), pp. 135–147.
- [23] M. KRONBICHLER AND K. KORMANN, *Fast matrix-free evaluation of discontinuous galerkin finite element operators*, ACM Transactions on Mathematical Software (TOMS), 45 (2019), pp. 1–40.

- [24] M. KRONBICHLER, D. SASHKO, AND P. MUNCH, *Enhancing data locality of the conjugate gradient method for high-order matrix-free finite-element implementations*, arXiv preprint arXiv:2205.08909, (2022).
- [25] J. L. LIONS, Y. MADAY, AND G. TURINICI, *A “parareal” in time discretization of PDEs*, *Comptes Rendus de l’Académie des Sciences - Series I - Mathematics*, 332 (2001), pp. 661–668.
- [26] P. MUNCH, T. HEISTER, L. PRIETO SAAVEDRA, AND M. KRONBICHLER, *Efficient distributed matrix-free multigrid methods on locally refined meshes for fem computations*, (2022).
- [27] P. MUNCH, K. KORMANN, AND M. KRONBICHLER, *hyper. deal: An efficient, matrix-free finite-element library for high-dimensional partial differential equations*, *ACM Transactions on Mathematical Software (TOMS)*, 47 (2021), pp. 1–34.
- [28] W. PAZNER AND P.-O. PERSSON, *Stage-parallel fully implicit Runge–Kutta solvers for discontinuous Galerkin fluid simulations*, *Journal of Computational Physics*, 335 (2017), pp. 700–717.
- [29] B. S. SOUTHWORTH, O. KRZYSIK, AND W. PAZNER, *Fast solution of fully implicit Runge–Kutta and discontinuous Galerkin in time for numerical PDEs, part II: Nonlinearities and DAEs*, *SIAM Journal on Scientific Computing*, 44 (2022), pp. A636–A663.
- [30] B. S. SOUTHWORTH, O. KRZYSIK, W. PAZNER, AND H. D. STERCK, *Fast solution of fully implicit Runge–Kutta and discontinuous Galerkin in time for numerical PDEs, part I: the linear setting*, *SIAM Journal on Scientific Computing*, 44 (2022), pp. A416–A443.
- [31] R. A. VAN DE GEIJN AND J. WATTS, *Summa: Scalable universal matrix multiplication algorithm*, *Concurrency–Pract. Ex.*, 9 (1997), pp. 255–274.
- [32] G. WANNER AND E. HAIRER, *Solving ordinary differential equations II*, vol. 375, Springer Berlin Heidelberg, 1996.